Journal of Applied Fluid Mechanics, Vol. 11, No. 5, pp. 1163-1171, 2018.
Available online at www.jafmonline.net, ISSN 1735-3572, EISSN 1735-3645.
DOI: 10.29252/jafm.11.05.28011

Numerical Simulation of Mucus Clearance inside Lung Airways

J. Kori† and Pratibha

Department of Mathematics, Indian Institute of Technology Roorkee, Roorkee, Uttarakhand, 247667, India

† *Corresponding Author Email: jyotikorii@gmail.com, jotikdma@iitr.ac.in*

(Received May 17, 2017; accepted February 20, 2018)

ABSTRACT

Airway mucus is difficult to clear and to improve lung function clearance of mucus is necessary. The deep coughing, chest physiotherapy, high frequency chest wall oscillation etc. are some of the best methods to clear excessive mucus from lung airways. In this article we analysed the behavior of fluid flow between parallel walls , where both walls are porous and the flow is induced by the oscillation of these walls and pressure gradient; which is applicable for clearance of mucus from lung airways. Generalized couette flow is applicable to model the oscillation of parallel walls, however the laminar flow of viscous fluid is taken under consideration. The generalized Navier-Stokes equations are applied to make various hypotheses and finite difference scheme is used to solve the problem numerically. Effect of wall oscillation, wall porosity, pressure due to porous media on mucus clearance and particle aspect ratio on the deposition of nonspherical nanoparticles are analysed graphycally after simulating the problem on MATLAB R2013a by user defind code. Simulation show an excellent agreement of unsteady flow of viscous fluid at large values of time and significant correlation between pressure gradient and porosity of walls, frequency of wall oscillation and their imapct on mucus clearance are obtained. In addion it is observed that fluid and particle velocity are increased with the enhancement of media porosity, breathing frequency and aspect ratio. The aim of this paper is to study the influence of wall movement, wall porosity, pressure on wall, wall oscillating frequency on the clearance of mucus from lung airways.

Keywords: Cilia movement; Couette flow; Mathematical modeling; Mucus clearance; Porosity; Particle shape.

NOMENCLATURE

d	diameter of spherical particle of unite density	t	time
D_a	Darcy number	u_x	air velocity radial direction
d_i	inner diameter of alveolus	u_y	air velocity axial direction
d_o	outer diameter of alveolus	v_x	particle velocity radial direction
F_s	Forchheimer number	v_y	particle velocity axial direction
g_x	axial component of gravity	ρ_a	density of air
g_y	radial component of gravity	ρ_p	density of particles
k_f	stokes drag force	v	kinematic viscosity
P_l	particle load		

1. INTRODUCTION

There are two main natural mucus draining methods in the bronchial tree, first, mucociliary clearance and second is cough. The mucus layer coats the interior parts of human respiratory ducts (Fulford and Blake (1986)) and protects the airways against extrinsic attacks. It moves upward toward the oropharyngeal bifurcation after capturing the aerocontaminers, with the motion of the cilia (Lai *et al.* (2009), King (2006)). Cilia are hairlike object in the inner surface of airways, which vibrate to defend the walls against contaminated particles in the inhaling air. When we sleep, clearance efficiency is diminished and it enhanced during exercise. Consequently, ventilation rate plays an important role on mucus evacuation. So, there are two main selected phenomena to understand the structure of mucus distribution in the lungs (i) how it moves forward efficiently toward the trachea, and (ii) what is the effect of movement of this layer over air flow inside lung.

Mucus is a viscous fluid and due to propulsion caused by coughing both walls are oscillate in their own plane and cilia move in downward and up-ward directions; as a result, mucus and trapped particles move toward the trachea. This phenomena can be understood by unsteady couette flow. The couette flow is an ideal flow usually used to model shear-driven flows experienced in small motors, small channels and different small fluid systems. We assume cilia as a porous matrix and flow of mucus over it as a moving wall. The flow is induced by the movement of both walls and the pressure gradient. Generally, for very slow flow which is dominated by viscous effect, the Darcy model has been the basic approach employed. However, fluid transfer through high pressure, which can arise in various capillary networks is dominated by inertial drag effects. An elegant and robust methodology for this is the extension of the Darcy low Reynolds number drag force model to the Darcy-Forchheimer nonlinear model which includes a supplementary quadratic drag force term.

Additionally, inhaled aerosol mechanics is influenced by lower range Reynolds number, deformations of septal walls, and time dependent airflow patterns leading to irreversible kinematics within alveolar cavities during cyclic breathing (Haber *et al*. (2003)). Particles with diameter from 10 nm to 200 nm are ideal size to deposit in deep lung airways (Shah (2009)), while particle shape allows long skinny particles to orient with the tiniest diameter within the direction of air flow (align along their long axis) permitting them to deposit deep within the lung (Timbrell (1982)). For example carbon nanotubes (He *et al*. (2013)), nanofibers, nanowire, nanorod are needle-shaped particles which are presently used in various cosmetic products, may enter through skin in respiratory system (Ikegami *et al.* (2002)).

There are a few studies (Chang *et al*. (1988), van Vliet *et al.* (2005), Mazumder and Das (1992), Jiang and Grotberg (1993)), which reported that tube wall oscillation may enhance displacement of mucus during coughing. Some other studies (Johnson *et al.* (1991), Halpern and Grotberg (1993), Otis *et al.* (1993)) are applied couette flow inside lung because lung comprised a network of bifurcating airway tubes which are coated with a thin viscous film. Moreover, an analytical expression of couette flow and heat transfer through a composite system was presented in Kuznetsov (1998). Jones *et al*. (1995) studied isotope mucociliary clearance rates in Cystic Fibrosis subjects and found that the effective clearance occurred by increasing frequency of 10-15 Hz because at this frequency oscillated flow is highest. Additionally, Schlichting and Gersten (2003) presented a result of Navier-Stokes equations for the flow between two parallel plates without suction. A case for changeable pressure in the direction of flow of the system created eventually by Rouleau and Osterle (1995) and a study of the three dimensional flow and heat transfer along a flat plate by applying periodic suction done by Ger-sten and Gross (1974).

However, there were not many studies considering flow oscillation and particle transportation together through porous media. So the aim of this study is to fill this gap by using media porosity, wall oscillation, and aspect ratio of inhaled nanoparticles to understand the mechanism of airway clearance, where the inner walls of the lung tube from the mouth to the alveoli are coated with thin mucus layer. Flow of viscous fluid is forced by the oscillation of walls and sinusoidal pressure gradient through variable porous media. Generalized couette flow is applied to understand the mechanism of mucus flow and Navier Stokes equations are used to model the flow field. In addition, Newton's second law is used for particle trajectory. Finite difference numerical scheme is used to solve the problem and all the results are shown graphically after perform-ing computation work on MATLAB.

2. MATHEMATICAL MODEL

We suppose that the airways are subjected to oscillation due to periodic breathing or due to coughing and a sinusoidal pressure is applied on both the boundaries due to surrounding forces and porous media, which is applicable for propulsion of mucus over the cilia. In addition, cilia are assumed as porous matrix which is covered by thin layer of mucus. The graphical model can be visualized in Fig. 1. Fluid flow is determined by modeling this process as generalized unsteady couette flow. Initially there is no pressure gradient so we assumed that the velocities and stresses are zero at t=0.

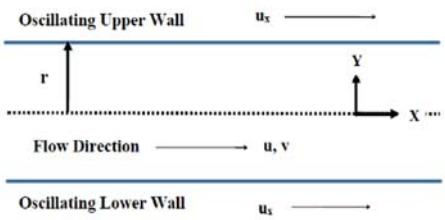

Fig. 1. Schematic Diagram for Oscillatory Walls

2.1 Governing Equations

Equation of continuity for air,

$$\frac{\partial \rho_a}{\partial t} + \frac{\partial \left(\rho_a u_x\right)}{\partial x} + \frac{\partial \left(\rho_a u_y\right)}{\partial y} = 0 \qquad (1)$$

Equation of continuity for particle,

$$\frac{\partial \rho_p}{\partial t} + \frac{\partial \left(\rho_p v_x\right)}{\partial x} + \frac{\partial \left(\rho_p v_y\right)}{\partial y} = 0 \qquad (2)$$

Equation of momentum in parallel (axial) direction,

$$\begin{aligned}&\frac{\partial u_x}{\partial t}+\frac{u_x}{\varepsilon}\frac{\partial u_x}{\partial x}+\frac{u_y}{\varepsilon}\frac{\partial u_x}{\partial y}\\&=-\frac{\varepsilon}{\rho_a}\frac{\partial p}{\partial x}+\nu\left(\frac{\partial^2 u_x}{\partial x^2}+\frac{1}{x}\frac{\partial u_x}{\partial x}+\frac{\partial^2 u_x}{\partial y^2}\right)\\&+\left(-\frac{\varepsilon\nu}{K}u_x+k_f\frac{\rho_p}{\rho_a}(v_x-u_x)-\frac{\varepsilon b}{K}u_x^2\right)\\&+g_x\left(\frac{\rho_p-\rho_a}{\rho_p}\right)\end{aligned}\qquad(3)$$

Equation of momentum in perpendicular (radial) direction,

$$\begin{aligned}&\frac{\partial u_y}{\partial t}+\frac{u_x}{\varepsilon}\frac{\partial u_y}{\partial x}+\frac{u_y}{\varepsilon}\frac{\partial u_y}{\partial y}\\&=-\frac{\varepsilon}{\rho_a}\frac{\partial p}{\partial y}+\nu\left(\frac{\partial^2 u_y}{\partial x^2}+\frac{1}{x}\frac{\partial u_y}{\partial x}+\frac{\partial^2 u_y}{\partial y^2}\right)\\&+\left(-\frac{\varepsilon\nu}{K}u_y+k_f\frac{\rho_p}{\rho_a}(v_y-u_y)-\frac{\varepsilon b}{K}u_y^2\right)\\&+g_y\left(\frac{\rho_p-\rho_a}{\rho_p}\right)\end{aligned}\qquad(4)$$

Where, K is the permeability, which depends on the porosity (ε) (Khanafer *et al*. (2012)). We used porosity in keeping with Ergun (1952) empirical formula together with the variable porousness of respiratory organ as follows:

$$K=\frac{\varepsilon^3 d_p^2}{150(1-\varepsilon)^2}\qquad(5)$$

$$\varepsilon=1-\frac{\rho_p d_p^2}{\left(d_0^2-d_i^2\right)}\qquad(6)$$

The equation of motion for particle trajectory: In axial direction,

$$\frac{\partial v_y}{\partial t}+v_y\frac{\partial v_y}{\partial y}+v_x\frac{\partial v_x}{\partial x}=\frac{F_d}{m}\qquad(7)$$

In radial direction,

$$\frac{\partial v_x}{\partial t}+v_y\frac{\partial v_x}{\partial y}+v_x\frac{\partial v_x}{\partial x}=\frac{F_{d_1}}{m}\qquad(8)$$

Different shape particles will make different drag forces with different particle terminal settling velocities; which might successively have an effect on the aerodynamic behavior of particles (Crowder *et al*. (2002)). A term known as particle shape factor (Sf) (Fuchs (1965)) is employed to figure out the transport and deposition of nonspherical particles (i.e. elongated shape particles). This term describes the ratio of the drag force on the non-spherical nanoparticles (F_d and F_{d_1}) to the corresponding drag force on the related spherical particles (f_d and f_{d_1}) with an equivalent volume by Hinds (1999). Mathematically, this relationship is expressed as below:

$$F_d=S_f f_d,\qquad F_{d_1}=S_f f_{d_1}\qquad(9)$$

Stokes drag forces on spherical particles are defined as follows:

$$\left.\begin{aligned}f_d&=k_f\left(u_y-v_y\right)\\f_{d_1}&=k_f\left(u_x-v_x\right),\end{aligned}\right\}\ \text{Where, } k_f=3\pi\mu C_f d_p\qquad(10)$$

Where, C_f is the correction factor for thin particles and is taken as 1.25. d_p is the diameter of nonspherical nanoparticles which depends upon the particle shape factor. Additionally, the individual particle shape factor (S_f) is gained from the subsequent formula as follows:

$$S_f=\frac{1}{3}\left(\frac{2}{S_{\parallel}}+\frac{1}{S_{\perp}}\right)\qquad(11)$$

Computation of the particle shape factor does not solely depends on particle shape but is also influenced by the coordination of a particle relative to the direction of air flow. Hence, nonspherical nanoparticle might adopt most popular coordinations within the airflow (Hinds (1999)). A straight-forward empirical idea for the dependency of S_f on particle coordination was popularized by Su and Cheng (2006). The authors described $S_{\perp}$ for those particles that are adjusted with their long axes (up-right to the air stream), however $S_{\parallel}$ for those whose long axes are aligned parallel to the air stream. From a mathematical point of view, $S_{\perp}$ and $S_{\parallel}$ is also determined by the subsequent equations:

$$\left.\begin{aligned}S_{\perp}&=\frac{\frac{8}{3}\left(\beta^2-1\right)\beta^{\frac{-1}{3}}}{\left(\frac{\left(2\beta^2-3\right)}{\left(\beta^2-1\right)^{\frac{1}{2}}}\right)\ln\left(\beta+\left(\beta^2-1\right)^{\frac{1}{2}}\right)+\beta}\\S_{\parallel}&=\frac{\frac{4}{3}\left(\beta^2-1\right)\beta^{\frac{-1}{3}}}{\left(\frac{\left(2\beta^2-1\right)}{\left(\beta^2-1\right)^{\frac{1}{2}}}\right)\ln\left(\beta+\left(\beta^2-1\right)^{\frac{1}{2}}\right)-\beta}\end{aligned}\right\}\ \beta>1\qquad(12)$$

where, β denotes the aspect ratio, which is the quantitative ratio of particle length to particle width, being β >> 1 for long nonspherical particles, β << 1 for extremely thin disks but for β = 0 there will be no existence of particle, since for this condition length and shape factor become 0. In this study we take 10 ≤ β ≤ 1000

for elongated nanoparticles. As per various theoretical and experimental studies, transportation of nonspherical particles in-side lung considerably disagree from that per-formed by spherical particles with classic aspect in same volume. To describe this specific condition the aerodynamic diameter is taken into account (Fuchs (1965)). The mathematical formulation of the aerodynamic diameter simplifies as follows:

$$d_p = d\sqrt{\left(\frac{\rho_p}{S_f \rho_0}\right)} \tag{13}$$

Where, ρ_0 is the unit density. Due to the deformation of alveolus wall and right heart pressure there is a time dependent sinusoidal pressure gradient within the alveolus, which can be outlined as follows,

$$-\frac{\partial p}{\partial y} = a_0 \sin \omega t, \qquad \omega = 2\pi f \tag{14}$$

Where, f is the breathing frequency.

2.11 Assumptions for Couette Flow

Assuming distance between both walls is 2r.

(i) For fully developed flow,

$$\frac{\partial u}{\partial x} = 0; \tag{15}$$

(ii) For unsteady generalized couette flow,

$$\left.\begin{matrix} \frac{\partial}{\partial t} \\ u_x \\ v_x \\ \frac{\partial p}{\partial x} \end{matrix}\right\} \neq 0 \tag{16}$$

$$\left.\begin{matrix} u_y \\ v_y \end{matrix}\right\} = 0 \tag{17}$$

2.12 Initial and Boundary Conditions

(i) Initial conditions at t=0,

$$\left.\begin{matrix} u_x \\ v_x \\ u_y \\ v_y \end{matrix}\right\} = 0 \tag{18}$$

(ii) Boundary conditions at t>0,

(a) Oscillation of top wall, when y=r:

$$u_x = u_0\left(1+\cos\left(2\pi f t\right)\right) \tag{19}$$

(b) Oscillation of bottom wall, when y=-r:

$$u_x = u_0\left(1+\cos\left(2\pi f t\right)\right) \tag{20}$$

3. METHODOLOGY

3.1 Transformation of the Governing Equations

Introducing the subsequent nondimensional quantities.

$$\begin{aligned} x^* &= \frac{x}{r}, y^* = \frac{y}{r}, p^* = \frac{\mathrm{Pr}^2}{\rho_a \nu^2}, t^* = \frac{t\nu}{r^2}, u^* = \frac{ur}{\nu}, \\ v^* &= \frac{vr}{\nu}, F_s = \frac{b}{r}, P_l = \frac{\rho_p}{\rho_a}, D_a = \frac{K}{r^2}, S_k = \frac{kr^2}{\nu}. \end{aligned} \tag{21}$$

We applied above nondimensional quantities in Eqs. (1)-(14) and got the following equations after dropping the asterisks (∗):

$$\frac{\partial u_x}{\partial x} = 0 \tag{22}$$

$$\frac{\partial v_x}{\partial x} = 0 \tag{23}$$

Momentum in axial direction,

$$\begin{aligned} &\frac{\partial u_x}{\partial t} = -\varepsilon \frac{\partial P}{\partial x} + \frac{\partial^2 u_x}{\partial y^2} \\ &+S_k P_l \left(v_x - u_x\right) - \frac{\varepsilon}{Da} - \varepsilon \frac{F_s}{Da} u_x^2 \end{aligned} \tag{24}$$

Momentum in radial direction,

$$\frac{\partial P}{\partial y} = \frac{1}{\varepsilon}\frac{r^3}{\nu^2} g_y \left(\frac{\rho_p - \rho_a}{\rho_p}\right) \tag{25}$$

Particle trajectory in parallel (axial) direction,

$$\frac{\partial v_x}{\partial t} = S_f S_k \frac{\left(u_x - v_x\right)}{m} \tag{26}$$

Particle trajectory in perpendicular (radial) direction,

$$u_x = v_x \tag{27}$$

3.2 Numerical Method

Finite difference scheme is a basic and less te-dious technique for a regular geometry. Therefore, the finite difference scheme is employed to solve the governing equations with central difference ap-proximation for all the spatial derivatives and for-ward difference approximation for time derivatives (Smith (1985)). To calculate the velocity of air ((u_y), (u_x)) and nonspherical nanoparticles ((v_y), (v_x)) a code is developed on MATLAB R2013a by setting the grid space as follows:

$$\begin{aligned} x_i &= i.\Delta x; \quad i = 0,1,2,3.....M, \qquad r_N = 1.0 \\ y_j &= j.\Delta y; \quad j = 0,1,2,3.....N, \\ t_k &= (k-1).\Delta t; \quad k = 1,2,3....O \end{aligned} \tag{28}$$

The discretization of axial velocity $u(x,y,t)$ is written as $u_x(x_i,y_j,t_k)$ or $((u_x)_{i,j})^k$ and also u_y, v_x, v_y

can be written similarly. The mesh dependency of the solution was additionally inspected for various grid sizes, i.e. 10x10, 15x15, 20x20, 30x30, and 40x40, in the axial and radial directions to figure out the flow field, but we found that the results remain consistent when the grid size is set 20x20 and above. So, the time step and grid space chose $\Delta t = 0.001$, $\Delta x = 0.05$ and $\Delta y = 0.05$ respectively. In addition, for computation following stability criteria is used.

$$\max\left[\frac{\Delta t}{\Delta x^2}\right] \leq 0.5 \tag{29}$$

Results are appeared to converge with the accuracy of order of 10^{-3}.

4. RESULTS AND DISCUSSION

In this article we modeled a horizontal channel whose both boundary walls are porous and subjected to oscillate along their own axis. The walls are 2r distance apart from each other with an incompressible unsteady laminar fluid flow be-tween them. Generalized couette flow, illustratively shown in Fig. 1, is a simplest close guess for periodic shear-driven flow met in the upper airways due to mucus overlay. The influence of the con-trolling limits on the flow velocity (for air, u and for particle, v) and pressure gradient (p) with respect to time (t) for different values of aspect ra-tio $10 \leq \beta \leq 1000$, porosity $0.6 \leq \varepsilon \leq 1$, frequency limit $0.2 \leq f \leq 1.2$ and time (t) is analysed in Figs. 2-6 (from Eqs. (22)-(27)), to observe the impact of dimensionless units. We use the follow-ing numerical values (Saini *et al*. (2017), Weibel (1964)) to solve the problem computationally.

$$v = 1.71*10^{-5} m^2/s, S_f = 1.54, \varepsilon = 0.6, r = 0.5\mu m,$$
$$m = 2*10^{-4} Kg/l, d = 50nm, f_p \leq 1.2hz, F_s = 1,$$
$$\rho_a = 1.145, \rho_p = 2.504*10^{10}, a_2 = 0.25 Kg/m^2 s^2.$$

4.1 Effect of Porosity on the Clearance of Mucus

Figures 2a and 2b depict the behavior of transient velocity of air (u) and particle (v) for different level of porosity ($0.6 \leq \varepsilon \leq 1$) at β=10, F_s=1 and f=1.2 with respect to t. It can be seen from Fig. 2a velocity of air is low at ε=0.6 and it increases when we increase ε from 0.6 to 1.0 and attains maximum velocity at ε=1. Further, along with wall due to oscillation velocity of air increases with the increment in ε (for thin mucus layer) via t, and when we go far from wall , velocity values reaches their steady state values after t=0.1. Additionally, velocity of particle is also increased (as shown in Fig. 2b) with the increment in ε from 0.6 to 1 via t and attains maximum velocity at ε=1. From these figures, it is clear that both velocities (for air, u and for particle, v) are affected by the increment in ε and it is interesting to observe that up to a particular time velocity of air increases and then time required to attains a steady state is unbiased with respect to the value of porosity.

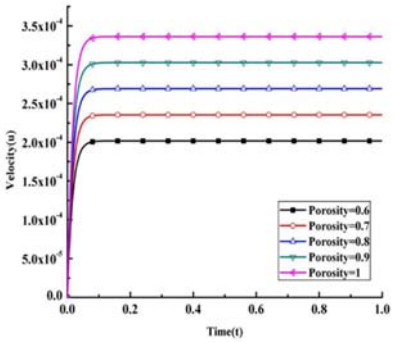

(a)

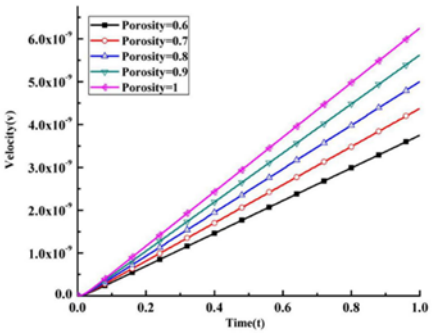

(b)

Fig. 2. Variation in (a) air velocity (u) (b) particle velocity (v), with respect to porosity ($0.6 \leq \varepsilon \leq 1$)

It can be correlated physically, as the void size or porosity increases breathing capacity increases which causes increment in air velocity. In either case, free flow of fluid is allowed a rise within the velocity of the fluid, which give propulsion and useful to clear thin layer of mucus.

4.2 Effect of Aspect Ratio on Particle Deposition

Figures 3a and 3b show the dimensional distribution of velocity at different level of aspect ratio ($10 \leq \beta \leq 1000$) at ε=0.60, F_s=1 and f=1.2 with respect to t. It is evident in Fig. 3a that velocity of air is low at β=10 and it increases when we increase particle β from 10 to 1000 and attains maximum velocity at β=1000. Velocity of air increases with the increment in β via t, and eventually reaches its steady state values after t=0.2. Here, it is interesting to note that the steady state of the air velocity delayed via t as value of β increased. While in Fig. 3b, velocity of particle increases with the increment in β from 10 to 1000 via t monotonically and attains maximum velocity at β=1000. It comes physical because the increment in air and particle velocity are caused by an enhancement in the aspect ratio of the particles. This physiological phenomenon is explained by the fact that particles are oriented along the air

movement and flow along the stream in downward direction as time in-creases, which means particles with low aspect ratio are deposited in former airways while particles with high aspect ratio have tendency to go deep inside the lung airways with air stream.

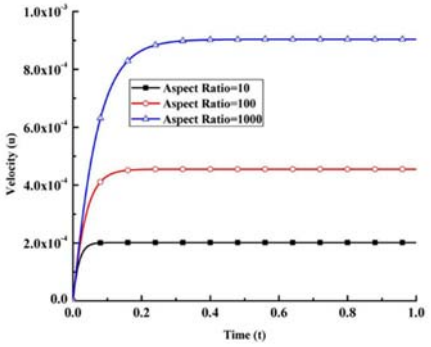

(a)

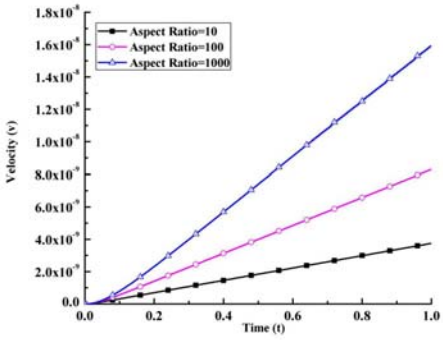

(b)

Fig. 3. Variation in (a) air velocity (u) (b) particle velocity (v) with respect to aspect ratio ($10 \leq \beta \leq 1000$)

4.3 Effect of Frequency on Wall Oscillation and Fluid Velocity

In Figs. 4a and 4b, we can see the impact of frequency ($0.2 \leq f \leq 1.2$) on fluid velocity (on air, u and on particle, v) at ε=0.60, F_s=1 and β=10 with respect to t. These figures show that the changes in fluid velocity occur due to the sinusoidal oscillation of wall caused by different frequency of breathing. It is observed that the magnitude of fluid velocity within the channel relies on the frequency of oscillation ($0.2 \leq f \leq 1.2$). In Fig. 4a, it can be seen that due to the increment in f from velocity (v) with respect to frequency ($0.2 \leq f \leq 1.2$). 0.2 to 1.2 increased velocity of air before t=0.1 and after that it becomes steady. Also, from Fig. 4b, it is observed that the velocity of particle increases gradually as f increases from 0.2 to 1.2 and attains maximum velocity at f=1.2. We can see the numerical values obtained after computation in Table 1, which depicts the transient velocity for air and particle via time for different value of wall frequencies. It is observed that air velocity increases initially, and become steady for large values of time for particular frequency, on the other hand the velocity of particle increases gradually with time.

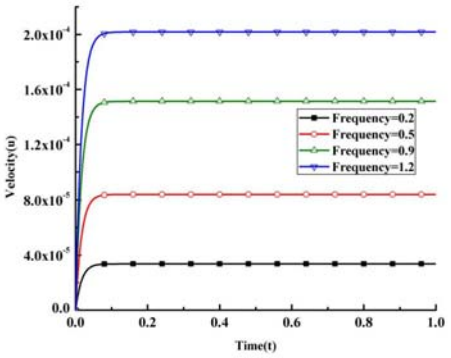

(a)

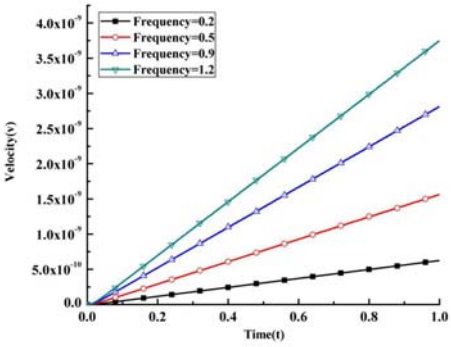

(b)

Fig. 4. Variation in (a) air velocity (u) (b) particle velocity (v) with respect to frequency ($0.2 \leq f \leq 1.2$).

4.4 Effect of Porosity (ε) on Air Pressure (p)

The effect of wall porosity (ε) on air pressure (p) is shown in Fig. 5 via t at β =10, F_s=1, and f=1.2. We are presenting velocity profiles for generalized couette flow due to oscillation of both walls at $0.6 \leq \varepsilon \leq 1$. For all the cases,

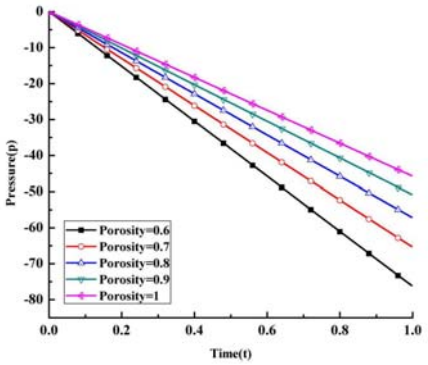

Fig. 5. Effect of porosity ($0.6 \leq \varepsilon \leq 1$) on air pressure (p)

the air pressure increases by decreasing ε=1.0 to 0.6 monotonically, since for low porosity pressure gradient is very high, which is responsible to remove thin mucus layer from air-ways and may improve lung function. We can see the numerical values obtained after numerical computation in Table 2. In this table pressure (p) for different values of porosity (ε) is shown with respect to time. It is noticed that pressure is increased as time and porosity decreased. This pressure is helpful to push the mucus forward. We plotted Fig. 5 for fluid velocity with different values of $0.6 \leq \varepsilon \leq 1$ and found consequent results. Increase level of pressure can often be visible on the whole length of the wall.

4.5 Comparison between Air Velocity Obtained Through Oscillatory Walls and Nonoscillatory Walls

Since lung is one of the main organ in respiration and its wall oscillates periodically during breath. Thus, we used a time dependent function to show oscillation of walls. Each wall oscillates to and fro along its axis. The effect ofwall oscillation on air velocity is depicted in Fig. 6 with respect to time (t) at β=10, F_s=1, f=1.2 and ε=0.60. The velocity of air (see Fig. 6) is largely affected when walls are os-cillating as compare to when walls are not oscillating along their axis. In addition, we found that the steady state of the air velocity is attained much earlier with nonoscillatory walls than oscillatory walls.

5. CONCLUSIONS

A problem of two dimensional unsteady couette flow of viscous fluid through oscillatory porous walls with sinusoidal pressure gradient (i.e. generalized couette flow) is investigated.

Porous walls are partially filled with a fluid. The flow of viscous fluid in the porous medium is modeled by the Naiver Stokes equation and solutions for the velocity profiles and the particle trajectory by newton second low with a set of initial and boundary conditions. Numerical pressure gradient in the axial direction are obtained graphically. The dependency of the parameters involved in the flow is discussed. The key findings of the present analysis are listed below.

(1) It is observed that for highly porous (ε =1) wall air and particle velocity increased, which is helpful to clear thin layer of mucus.

(2) For small aspect ratio (β=10) particles de-posited in former airways while for high aspect ratio (β=1000) particles have tendency to go deep inside lung with air stream.

(3) Viscous fluid velocity is proportional to the breathing frequency.

(4) For all the cases, the air pressure increases by decreasing media porosity ε from 1 to 0.6 monotonically, which is responsible to remove mucus from airways and may improve lung function.

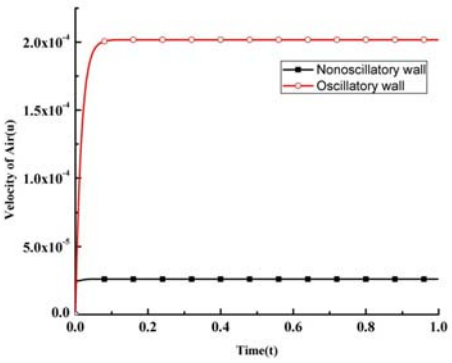

Fig. 6. A comparison of air velocity (u) between oscillatory walls to nonoscillatory walls at ε =0.6 and β =10

Table 1. Variation in velocities (u,v) via time (t) for different values of wall frequency (f)

	f=0.2		f=0.5		f=0.9		f=1.2	
time (t)	u(10^{-5})	v (10^{-9})	u(10^{-5})	v (10^{-9})	u(10^{-4})	v (10^{-9})	u(10^{-4})	v (10^{-9})
0.1	3.97423	0.626448	9.93324	0.156576	1.78686	0.281661	2.38078	0.375287
0.2	3.97930	0.137860	9.94590	0.344570	1.78913	0.619838	2.38382	0.825869
0.3	3.97931	0.213091	9.94593	0.532602	1.78914	0.958082	2.38383	0.127654
0.4	3.97932	0.288322	9.94595	0.720634	1.78914	0.129633	2.38383	0.172721
0.5	3.97933	0.363552	9.94597	0.908666	1.78915	0.163457	2.38384	0.217789
0.6	3.97933	4.38783	9.94598	1.09670	1.78915	1.97282	2.38384	2.62856
0.7	3.97934	5.14013	9.94600	1.28473	1.78915	2.31106	2.38384	3.07923
0.8	3.97935	5.89244	9.94602	1.47276	1.78915	2.64930	2.38385	3.52990
0.9	3.97935	6.64474	9.94603	1.66079	1.78916	2.98755	2.38385	3.98058
0.998	3.97936	7.38200	9.94605	1.84507	1.78916	3.31903	2.38386	4.42223

(5) We can say, other results and comparison of oscillatory wall to nonoscillatory wall validate our assumption that during cough and high frequency breath airways are oscillating and applicable for clearance of mucus.

Results obtained in this article regarding mu-cus clearance through circular tube whose walls are porous and oscillating along their own axis, can be helpful to understand mucus evacuation, movement of mucus towards the trachea, conditions of chronic obstructive pul-monary disease (COPD), emphysema, asthma, chronic bronchitis etc.. Moreover, the concept of generalized couette flow can be applied on other body parts where oscillation occur i.e. flow of blood through vein inside heart, flow through anal etc. and all the natural and real life phenomena where both walls are moving or oscillating along their own plane. Although, the present study is limited with upper air-ways. It is worth extending the study to lower airways or whole lung generations which may lead to a more general solution. Additionally, we can take other cases such as the movement of only one wall, when there is no pressure gradient etc. That may constitute a further work.

ACKNOWLEDGMENTS

The authors would like to thank the reviewers for their constructive comments, which have helped to improve the paper. One of the author, Jyoti Kori, is very thankful to Ministry of Human Resource Development India (Grant Code:- MHR-02-23-200-44) for financial provision and support while writing this manuscript.

Table 2. Variation in pressure (p) via time (t) for different values of wall porosity (ε)

	ε=0.6	ε=0.7	ε=0.8	ε=0.9	ε=0.9
t	p	p	p	p	p
0.1	-7.6346909	-6.5440208	-5.7260182	-5.0897939	-4.5808145
0.2	15.269382	-13.088042	-11.452036	-10.179588	-9.1616291
0.3	-22.904073	-19.632062	-17.178055	-15.269382	-13.742444
0.4	-30.538764	-26.176083	-22.904073	-20.359176	-18.323258
0.5	-38.173455	-32.720104	-28.630091	-25.44897	-22.904073
0.6	-45.808145	-39.264125	-34.356109	-30.538764	-27.484887
0.7	-53.442836	-45.808145	-40.082127	-35.628558	-32.065702
0.8	-61.077527	-52.352166	-45.808145	-40.718352	-36.646516
0.9	-68.712218	-58.896187	-51.534164	-45.808145	-41.227331
0.998	-76.041522	-65.178447	-57.031141	-50.694348	-45.624913

REFERENCES

Chang, H., M. Weber, and M. King (1988). Mucus transport by high pusle rate non symmetrical oscillatory air flow. *Journal of Applied Physiology* 65(3), 1203–1209.

Crowder, T., J. Rosati, J. Schroeter, A. Hickey, and T. Martonen (2002). Fundamental effects of particle morphology on lung delivery: predictions of stokes' law and the particular relevance to dry powder inhaler formulation and development. *Pharmaceutical Research* 19(3), 239–45.

Ergun, S. (1952). Fluid flow through packed columns. *Journal of Chemical Engineering Progress* 48(2), 89–94.

Fuchs, N. (1965). *The mechanics of aerosols*, Volume 91. John Wiley and Sons Ltd.

Fulford, G. and J. Blake (1986). Mucociliary transport in the lung. *Journal of Theoretical Biology* 121(4), 381–402.

Gersten, K. and J. Gross (1974). Flow and heat transfer along a plane wall with periodic suction. *Journal of Applied Mathematics and Physics* 25(3), 399–408.

Haber, S., D. Yitzhak, and A. Tsuda (2003). Gravitational deposition in a rhythmically expanding and contracting alveolus. *Journal of Applied Physiology* 95(2), 657–671.

Halpern, D. and J. Grotberg (1993). Surfactant effects on fluid-elastic instabilities of liquid-lined flexible tubes: a model of airway closure. *ournal of Biomechanical Engineering* 115(3), 271–277.

He, H., L. Pham-Huy, P. Dramou, D. Xiao, P. Zuo, and C. Pham-Huy (2013). Carbon nanotubes: Applications in pharmacy and medicine. *BioMed Research International*, 12.

Hinds, W. (1999). *Aerosol Technology, Properties, Behaviour, and Measurement of Air-borne Particles*, Volume 20. John Wiley and Sons Inc.

Ikegami, K., Y. Kawashima, H. Takeuchi, H. Yamamoto, N. Isshiki, D. Momose, and K.

Ouchi (2002). Improved inhalation behavior of steroid ksr-592 in vitro with jethaler by polymorphic transformation to needle-like crystals (beta-form). *Pharmaceutical Research* 19(10), 1439–1445.

Jiang, Y. and J. Grotberg (1993). Bolus contaminant dispersion in oscillatory tube flow with conductive walls. *ournal of Biomechanical Engineering* 115(4A), 424–431.

Johnson, M., R. Kamm, L. Ho, A. Shapiro, and T. Pedley (1991). The nonlinear growth of surface-tension-driven instabilities of a thin annular film. *Journal of Fluid Mechanics* 233, 141–156.

Jones, R., R. Lester, and N. Brown (1995). Effects of high pulse rate chest wall compression on respiratory system mechanics in nor-mal and cystic fibrosis patients. C*anadian Respiratory Journal* 2(1), 40–46.

Khanafer, K., K. Cook, and A. Marafie (2012). The role of porous media in modeling fluid flow within hollow fiber membranes of the total artificial lung. *Journal of Porous Media* 15(2), 113–122.

King, M. (2006). Physiology of mucus clearance. *Paediatric Respiratory Reviews* 7S(1), S212–S214.

Kuznetsov, A. (1998). Analytical investigation of couette flow in a composite channels partially filled with a clear fluid. International *Journal of Heat Mass Transfer* 41(16), 2556–2560.

Lai, S. K., Y. Wang, D. Wirtz, and J. Hanes (2009). Micro- and macrorheology of mucus. *Advanced Drug Delivery Reviews* 61(2), 86–100.

Mazumder, B. and S. Das (1992). Effect of boundary reaction on solute dispersion in pulsatile flow through a tube. *Journal of Fluid Mechanics* 239, 523–549.

Otis, D., M. Johnson, T. Pedley, and R. Kamm (1993). Role of pulmonary surfactant in airway closure: a computational study. *Advanced Drug Delivery Reviews* 75(3), 1323–33.

Rouleau, W. and J. Osterle (1995). The application of finite difference methods to boundary-layer type flows. *Journal of the Aeronautical Sciences* 22(4), 249–254.

Saini, A., V. Katiyar, and Pratibha. (2017). Two-dimensional model of nanoparticle deposition in the alveolar ducts of the human lung. *Applications and Applied Mathematics* 12(1), 305–318.

Schlichting, H. and K. Gersten (2003). *Boundary-layer theory*. McGraw-Hill, New York.

Shah, S. (2009). *Numerical simulation of particle adhesion dynamics for applications in Nanomedicine and Biosensing*. Ph. D. thesis, The University of Texas, Arlington.

Smith, G. (1985). Numerical solution of partial differential equations.

Su, W. and Y. Cheng (2006). Deposition of fiber in a human airway replica. *Journal of Aerosol Science* 37(11), 1429–1441.

Timbrell, V. (1982). Deposition and retention of fibres in the human lung. A*nnals Of Occupational Hygiene* 26(1), 347–369.

van Vliet, P., E. Ellis, and J. Hila (2005). The effect of angle and oscillation on mucous sim-ulant speed in flexible tubes. *Physiotherapy Research International* 10(3), 125–133.

Weibel, E. (1964). Two-dimensional model of nanoparticle deposition in the alveolar ducts of the human lung. *American Physiological Society* 2(1), 285–308